Impact of volume constraint and weighting factors of the electric field on topology optimization of electrodes: application to dielectrophoresis (DEP)-based devices

Abdenbi MOHAND-OUSAID[1], Abdullah ABDELRAHEEM[1],
Abbas HOMAYOUNI-AMLASHI[1] and Aude BOLOPION[1],

***Abstract*— The shape of electrodes is a key design parameter in dielectrophoresis (DEP)-based devices, directly influencing the DEP forces induced by applied voltage to the electrodes. These forces find application in medical therapy devices, particularly in tasks such as cell manipulation, sorting and separation. In these applications, it is essential to control the direction and the magnitude of the DEP forces. To address this challenge, this paper proposes to use topology optimization to design the shape of the electrodes. Building upon our previous research, we investigate the influence of the volume fraction constraint and the weighting factors of the electric field components along X and Y axes on the resulting electrode layouts and their corresponding DEP force performances. To this purpose, a case study has been defined as trapping particles inside a desired convergence zone in a fluid stream inside a microchannel. A series of numerical simulations were conducted to evaluate the influence of the volume constraint and weighting factors. The results show that for each set of parameters the methodology enables the generation of electrode layouts that effectively direct the DEP forces to trap the targeted particles. Beyond this, The results show that, for this type of problem, it is not advantageous to impose a volume constraint. The optimization process implicitly identifies the volume that achieves the best trade-off between material distribution and DEP forces.**

***Index Terms*— Dielectrophoresis (DEP) forces, Electrode design, Topology optimization**

I. INTRODUCTION

Cell sorting techniques play a critical role in numerous biological and medical applications, enabling the identification, characterization, and purification of specific cell subpopulations. Such methods are essential for various research and clinical protocols, from cancer therapies to studying signaling between blood cells [1]. In this framework, several sorting techniques have been described in the literature [2]–[7]. They can be classified in two main categories: active and passive [2]. Active ones separate cells by using external fields such as acoustic, electric, magnetic or optic, while passive ones separate cells through inertial forces, filters or adhesion mechanisms. Among these techniques, dielectrophoresis (DEP) is of particular interest because it acts on neutral but polarized cell [5] and does not require any damaging chemical treatment. This technique lies on a DEP phenomena that induces unbalanced charges on the surface of living cells. When these cells are suspended in a medium of different dielectric characteristic, they become electrically polarized. Due to the difference between the polarity of the cells and the medium, positive or negative DEP will occur. In this case, the generated force pulls the cells in the direction of increasing electrical field (positive DEP) or pushes the cells in the direction of decreasing electrical field (negative DEP) [2]. The cell sorting devices, called also lab on a chip devices, combine this force with fluidic for accurate separation of cells of interest from other cells.

Although, cell-sorting devices bring a significant progress in cell separation, their development remains challenging in particular the design of their electrodes. The abundant papers tell us how much importance researchers attached to solve this issue. Various empirical electrode shapes are proposed including parallel [8], interdigitated [9], castellated [10], quadrupole [11], annular [12], oblique [13], curved [14], etc. A brief review of each of these designs is reported in [15]. Recently, optimization approaches have been used to design more efficient electrodes. The optimization methods include investigative approach on the basic shapes of the electrodes like rectangular and trapezoidal [16], different placement of rectangular electrodes [17], shape optimization using genetic algorithm [18], [19] and microelectrode discretization [20]. A major limitation of these optimization approaches lies in their high computational cost, which requires the use of large rectangular elements to discretize the electrode design domain. This restricts the diversity of the obtained geometry of the electrodes. As an alternative, Yoon et al. [5] applied topology optimization to design the shape of electrodes. Although this method offers significant potential for generating complex and efficient geometries, it remains limited by the implicit computation of sensitivities, which affects its computational efficiency.

To overcome the above-mentioned limitation, we recently proposed an explicit formulation of the sensitivities of the dielectrophoretic force (objective function) to facilitate the topology optimization of electrode shapes using a gradient-based algorithm [21]. To validate this approach, the trapping of artificial objects within a microfluidic channel was considered. The primary objective was to identify electrode topologies that outperform the conventional U-shaped design. A mathematical formulation was developed, optimized for two distinct volume constraints (0.3 and 0.4), and subsequently analyzed through numerical simulations and validated experimentally. The results clearly demonstrated the superior performance of the optimized topologies over the conventional U-shaped electrodes, particularly in terms of particle convergence to the trapping region.

[1] Université Marie et Louis Pasteur, SUPMICROTECH, CNRS, institut FEMTO-ST, F-25000 Besançon, France {abdenbi.mohand}@femto-st.fr

Building upon our previous work [21], this paper investigates the impact of the volume fraction constraint and weighting factors of the electric field components along X and Y axes on the resulting 2D electrode layouts and their corresponding DEP force performances. This is essential to further demonstrate the interest of topology optimization of electrodes shapes and understand how these factors influence the electric field distribution, which governs the magnitude of the DEP forces.

II. Topology Optimization SIMP method

This section briefly recalls the main concept behind the topology optimization-based density approach. This approach, especially the SIMP (Solid Isotropic Material with Penalization) method, is a design methodology aiming to find an optimal structure within a limited design domain subjected to one or several constraints. Unlike classical methods, this powerful mathematical method consists of distributing material in areas where it is necessary and removing it from areas where it is not needed [22]. To this end, the method combines finite element formulation and penalization power law to make material intermediate density unattractive and, therefore, avoid the 0-1 problem of classical topology optimization process. For more details readers can refer to a reference book entitled "Topology Optimization: Theory, Methods and Applications" [22], where the theoretical foundations and applications of this approach have been comprehensively described and extensively discussed. Solid mechanics has historically been the primary field of application of topology optimization, where the main objectives are weight reduction and stiffness enhancement. Over time, topology optimization has progressively expanded to a wide variety of applications, ranging from photonics [23], optics [24], magnetism [25], electronics [26], electro-active polymers [27], shape memory polymers [28], piezoelectric actuators [29]–[33] to electrostatic actuators [5], [21], [34].

III. Dielectrophoretic force Modeling

This section briefly reminds the dielectrophoretic force modeling derived in [21]. Any neutral particle subjected to a non-uniform electric field will experience an electrostatic force due to Maxwell's stress tensor. For a spherical particle, Maxwell's stress tensor generates a dielectrophoretic (DEP) force that can be expressed as [35], [36]

$$F_{DEP} = 2\pi\varepsilon_m r^3 Re(f_{CM})\nabla|E|^2 \tag{1}$$

in which r is the radius of the particle, ε_m is the permittivity of the medium (fluid), ∇ is the vector differential operator and E is the electric field,

$$E = -\nabla\Phi \tag{2}$$

where Φ is the potential field applied to the electrodes. In addition, in equation (1), f_{CM} is the Clausius Mossotti factor that can be calculated as

$$f_{CM} = \frac{\varepsilon_p^* - \varepsilon_m^*}{\varepsilon_p^* + 2\varepsilon_m^*}$$
$$(\varepsilon_p^* = \varepsilon_p - j\frac{\sigma_p}{\omega}, \varepsilon_m^* = \varepsilon_m - j\frac{\sigma_m}{\omega}) \tag{3}$$

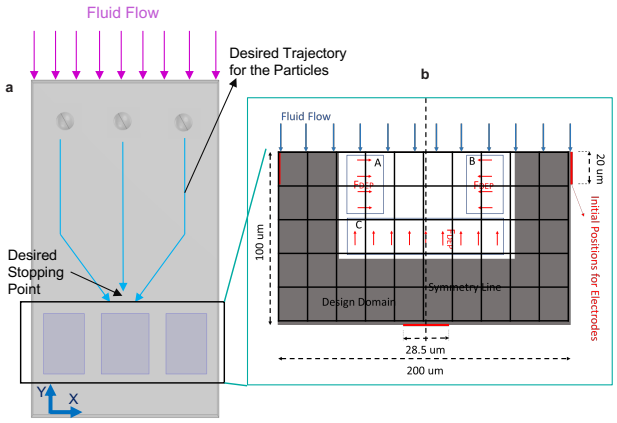

Fig. 1. Formulation of the particle trapping problem in a microfluidic channel. a) Desired trajectories of particles within the channel (top view). b) Representation of the design domain and its dimensions, the mesh and the boundary conditions.

where ε_p and σ_p are the permittivity and the conductivity of the particle. σ_m is the conductivity of the fluid, ω is the frequency of the AC potential and $\{\ ^*\ \}$ refers to the complex form of ε_p and ε_m.

A quick analysis of equation (1) reveals an important observation. For a given particle radius and a constant frequency, the DEP force magnitude is governed by the squared gradient of the electric field (i.e., $\nabla|E|^2$). Based on this observation, it is clear that, for a given application such as particle trapping, optimizing the shape of the electrodes is essential for enhancing the DEP force.

IV. Trapping problem formulation

Figure 1 illustrates the formulation of the particle trapping problem. For simplicity, only the region subjected to optimization is depicted. The remaining components of the microfluidic device namely, the fluid inlet and outlet, as well as the entrance electrode network used to center the particles are excluded. Ideally, any particle driven by the fluid through the microchannel should converge and then immobilized within a designated trapping zone, as illustrated in Fig. 1.a. Physically, this implies that the electrodes must generate appropriate electric fields capable of inducing dielectrophoretic (DEP) forces that redirect and guide the particle from a random initial location toward the convergence zone. As shown in Fig. 1.b, establishing a stable trap requires two opposing DEP forces along the X axis and an additional DEP force along the Y axis. Depending on the particle's initial position, the first two forces will steer it either from left to right or right to left, while the third force counteracts the fluid's drag force.

The simultaneous application of these DEP forces creates a funnel that drives the particle naturally toward the desired trapping zone. To achieve this funnel mechanism through electrode design, the optimization process must shape the electrodes to generate strong DEP forces in the targeted regions. The objective is therefore to identify a topology that maximizes the gradient of the electric field in the sub regions "A", "B", and "C" as illustrated in Fig. 1.b. Given this configuration, the optimization problem can be formulated as the minimization of the following objective

function (which is equivalent to the maximization of the DEP forces):

$$J = -W_x\Big(\int_{\Omega_A} |\frac{\partial}{\partial x}(E_x^2+E_y^2)|d\Omega - \int_{\Omega_B} |\frac{\partial}{\partial x}(E_x^2+E_y^2)|d\Omega\Big) - W_y\int_{\Omega_c} |\frac{\partial}{\partial y}(E_x^2+E_y^2)|d\Omega \quad (4)$$

where J is formulated as the weighted negative sum of the electric field gradients corresponding to each zone. W_x et W_y are the weighting factors with $W_x + W_y = 1$ and Ω is the design domain. This optimization is subjected to a volume constraint that defines the quantity of conductive material to distribute within the design domain. In practice, it is expressed as the ratio "*VolFrac*" between the volume of the distributed material V_0 and the total volume of the design domain V, which is by definition strictly bounded between 0 and 1.

The minimization process of J under the volume fraction constraint is repeated iteratively until all design variables converge either towards a value close to "0", corresponding to fluid regions, or towards a value close to "1", indicating the presence of electrode material. The finite element discretization of the design domain, the derivation of the elementary dielectric matrix, the interpolation scheme of the permittivity between fluid and material, the assembly of the global dielectric matrix and the sensitivity analysis are investigated in detail in [21]. Readers are referred to this work for further information.

As part of the logical progression of our previous research [21], we aim here to investigate the impact of the volume fraction constraint and the weighting factors on the electric field distribution, which governs the magnitude of the DEP forces. It is worth to notice that these parameters are chosen intuitively in the previous study.

V. Analysis of the impact of volume fraction and weightings factors

To evaluate the impact of the volume fraction and the weighting factors, the minimization of the objective function J was carried out using several sets of values of *VolFrac*, W_x and W_y as shown in Tab. I. Each cell of the table presents a unique combination of *VolFrac*, W_x and W_y. In one hand, 10 combinations of *VolFrac* are considered from 0.1 to 1 with an increment of 0.1. In the other hand, 11 combinations of W_x and W_y are considered from (0,1) to (1,0) with an increment of (0.1,-0.1). Due to the symmetry of the electrodes design domain given in Fig. 1.b, only 65 combinations were tested, as indicated in the Tab. I by crossed boxes. It is worth noting that the value of *VolFrac* starts at 0.1 in order to deposit a minimal amount of material (electrode), and ends at 1, which corresponds to a case where the volume constraint is fully relaxed.

Figures 2, 3, 4 and 5 illustrate the results of the optimization for four cases of parameter combination (*VolFrac*=(1,1,1,1), W_x=(0.2,0.4,0.5,0.8) and W_y=(0.8,0.6,0.5,0.2)). They present the obtained electrode

TABLE I
Value sets of *VolFrac*, W_x and W_y

	1		2		3		4		5		6		7		8		9		10		11	
VolFrac	**No**	**Wx=0 Wy=1**	**No**	**Wx=0.1 Wy=0.9**	**No**	**Wx=0.2 Wy=0.8**	**No**	**Wx=0.3 Wy=0.7**	**No**	**Wx=0.4 Wy=0.6**	**No**	**Wx=0.5 Wy=0.5**	**No**	**Wx=0.6 Wy=0.4**	**No**	**Wx=0.7 Wy=0.3**	**No**	**Wx=0.8 Wy=0.2**	**No**	**Wx=0.9 Wy=0.1**	**No**	**Wx=1 Wy=0**
0.1	1.1	☒	2.1	☒	3.1	☒	4.1	☒	5.1	☒	6.1	☒										
0.2	1.2	☒	2.2	☒	3.2	☒	4.2	☒	5.2	☒	6.2	☒										
0.3	1.3	☒	2.3	☒	3.3	☒	4.3	☒	5.3	☒	6.3	☒										
0.4	1.4	☒	2.4	☒	3.4	☒	4.4	☒	5.4	☒	6.4	☒										
0.5	1.5	☒	2.5	☒	3.5	☒	4.5	☒	5.5	☒	6.5	☒										
0.6	1.6	☒	2.6	☒	3.6	☒	4.6	☒	5.6	☒	6.6	☒										
0.7	1.7	☒	2.7	☒	3.7	☒	4.7	☒	5.7	☒	6.7	☒										
0.8	1.8	☒	2.8	☒	3.8	☒	4.8	☒	5.8	☒	6.8	☒										
0.9	1.9	☒	2.9	☒	3.9	☒	4.9	☒	5.9	☒	6.9	☒										
1.0	1.10	☒	2.10	☒	3.10	☒	4.10	☒	5.10	☒	6.10	☒										

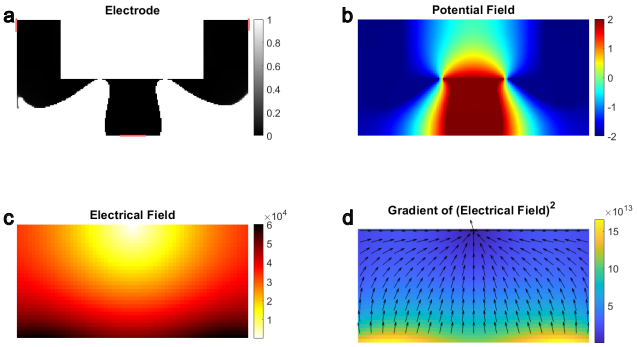

Fig. 2. MATLAB topology optimization results for the case $VolFrac$=1, W_x=0.2 and W_y=0.8. a) Obtained electrode topology. b) Potential field. c) resulted electrical field. d) Gradient of electrical field. The arrows are showing the DEP forces direction.

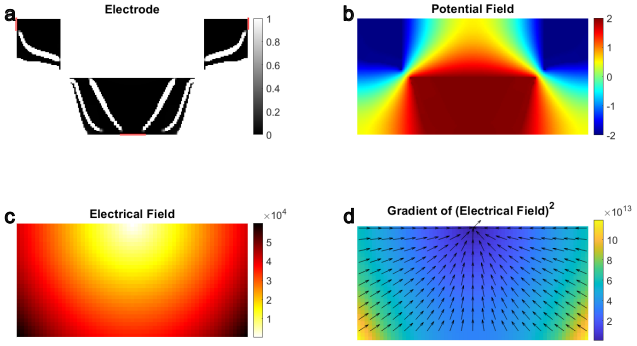

Fig. 3. MATLAB topology optimization results for the case $VolFrac$=1, W_x=0.4 and W_y=0.6. a) Obtained electrode topology. b) Potential field. c) resulted electrical field. d) Gradient of electrical field.

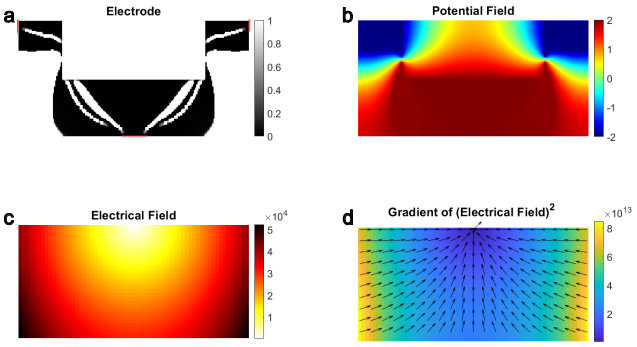

Fig. 4. MATLAB topology optimization results for the case $VolFrac$=1, W_x=0.5 and W_y=0.5. a) Obtained electrode topology. b) Potential field. c) resulted electrical field. d) Gradient of electrical field.

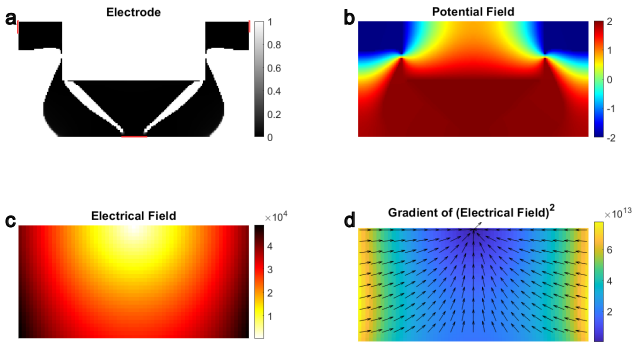

Fig. 5. MATLAB topology optimization results for the case $VolFrac$=1, W_x=0.8 and W_y=0.2. a) Obtained electrode topology. b) Potential field. c) resulted electrical field. d) Gradient of electrical field.

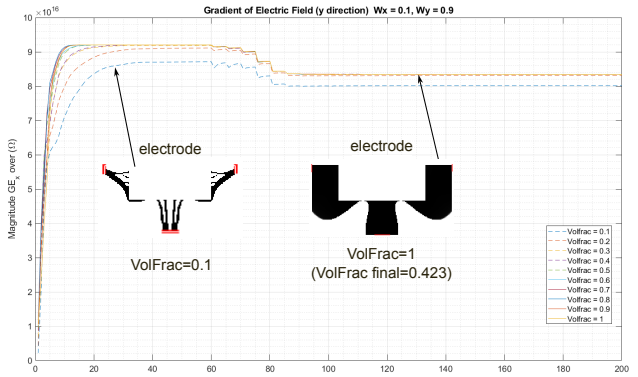

Fig. 6. Gradient of the electric field in Y direction with respect to $VolFrac$ that varies from 0.1 to 1 while W_x and W_y are set to (0.1 and 0.9). The curves are plotted as a function of the optimization iterations.

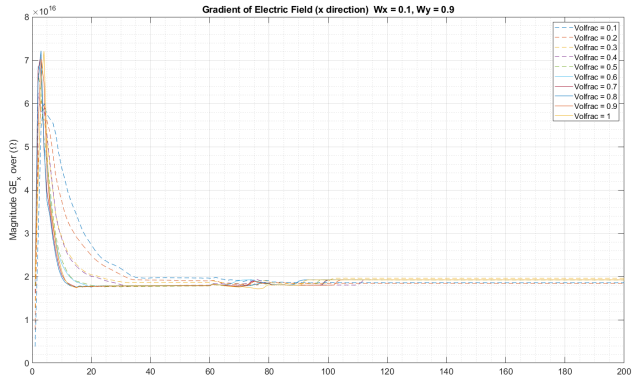

Fig. 7. Gradient of the electric field in X direction with respect to $VolFrac$ that varies from 0.1 to 1 while W_x and W_y are set to (0.1 and 0.9). The curves are plotted as a function of the optimization iterations.

topology, the potential applied to each electrode, the resulting electric field, and the electric field gradient, which provides an image of the DEP forces. For each case, it is clear that the DEP forces converge to the center and toward the inverse direction of the fluid flow as shown by the normalized arrows. This is in accordance with the defined directions in the formulation given in Fig. 1.

Figures 6, 7, 8 and 9 show the evolution of the gradient of the electrical field (along X and Y axes) for two combinations of W_x and W_y (0.1,0.9 and 0.2,0.8 respectively) with respect to $VolFrac$ that goes from 0.1 to 1 with an increment of 0.1. The analysis of all combinations shows that, regardless of the weighting factors, the highest gradient is generated when the volume constraint is set to 1 (see Figs. 6 and 8). A similar behavior is also observed for the other combinations of weighting factors, with only minimal difference in the final volume fraction when the volume constraint is set to 1. These results highlight that topology optimization algorithm has a systematical ability to converge to a solution with an optimal volume fraction when $VolFrac$ is set to 1. This is a remarkable feature of the optimization algorithm which identifies the most effective $VolFrac$ value. For example, the optimal volume fractions corresponding to the cases presented in Figs. 6 and 8 are 0.423 and 0.461, respectively. These results demonstrate that the algorithm reaches solutions

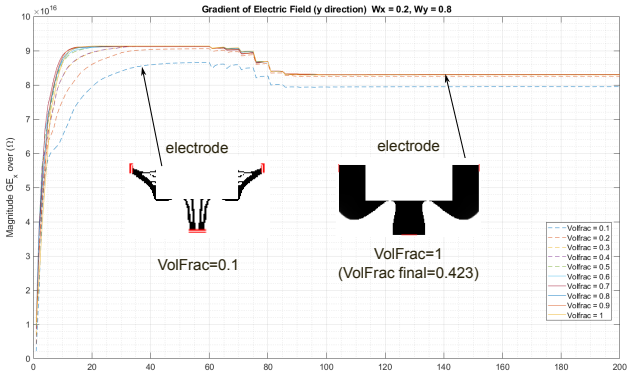

Fig. 8. Gradient of the electric field in Y direction with respect to *VolFrac* that varies from 0.1 to 1 while W_x and W_y are set to (0.2 and 0.8). The curves are plotted as a function of the optimization iterations.

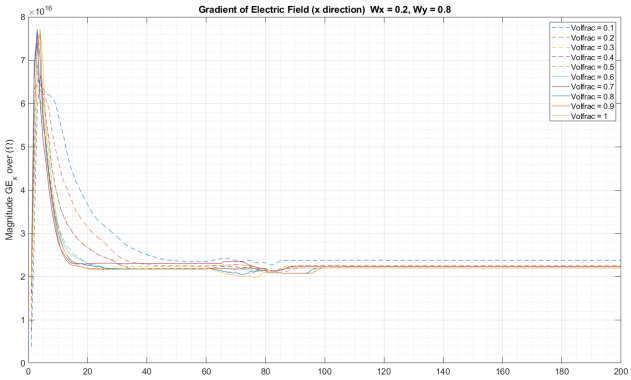

Fig. 9. Gradient of the electric field in X direction with respect to *VolFrac* that varies from 0.1 to 1 while W_x and W_y are set to (0.2 and 0.8). The curves are plotted as a function of the optimization iterations.

that maximize (or minimize) the desired output.

This result is initially challenging to predict, but it can be interpreted retrospectively by relying on the nature of the physics of the trapping problem. Indeed, the DEP forces induced by a non-uniform electrical field are generated by three electrodes. These electrodes, initially interconnected within the design domain (see red boundary conditions in Fig. 1.b), must be automatically separated by the algorithm to avoid a short circuit. Using a volume constraint of 1 relaxes the volume constraint, allowing the algorithm to automatically search for the optimal volume.

Furthermore, the impact of parameters W_x and W_y, regardless to volume fraction, is evident from the result shown in Figs. 2.d, 3.d, 4.d and 5.d. These parameters serve mainly to balance the DEP forces between the X and Y directions. When $W_x < W_y$ the DEP forces generated along the Y axis are stronger than those along X axis, and vice versa. Moreover, the pairs of Figs.(6,7) and (8,9) illustrate the complementarity of the generated DEP forces along X and Y axes respecting the primarily condition $W_x + W_y$=1. The increase in forces along the Y direction automatically reduces the forces along the X direction, and vice versa.

When considering the combined effects of the volume fraction and the weighting factors, the two configurations presented in Figs. 3 and 4 exhibit optimal particle trapping performance among the other configurations. In addition, these configurations require less than 5 volts,

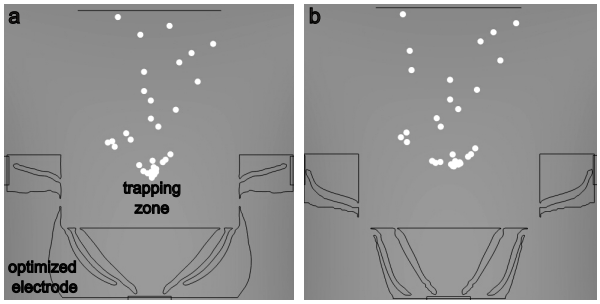

Fig. 10. Numerical simulation of the optimal electrodes in COMSOL.

thus significantly minimize particle exposure to the electric field. Their simulation in COMSOL under a fluid stream demonstrate their ability to deviate particles along the channel and drive them toward the desired trapping zone as it is clearly shown in Fig. 10.

VI. Conclusion

In conclusion, this paper demonstrates the interest of topology optimization as a methodological tool for designing electrodes shapes in DEP-based devices. By exploring the impact of the volume fraction and the weighting factors, the paper shows that the optimization process successfully generate topologies that direct DEP forces to trap particles in a desired region within the microfluidic channel. The results analysis highlights that imposing a volume fraction constraint is not beneficial in dielectrophoresis applications. Indeed, the optimization process identifies naturally the optimal volume fraction that balances material distribution with respect to the desired DEP force performances. The results highlight also the impact of the weighting factors that permit to balance the DEP forces along X and Y axes. A compromise between these factors allows, on one hand, to counterbalance the drag forces due to the fluid stream, and on the other hand to form a funnel that deviates particles from right to left and from left to right toward the desired trapping region. Future works will focus on the experimental validation of the optimized electrodes.

Acknowledgment

This work has been supported by the Marie and Louis Pasteur university Chrysalide project CREATURS and CIFRE N 2021/0039. This work has also been supported by (i) the BioImp project funded by EU through the European Regional Development Fund of the Region BFC (no. BFC000802) and (ii) the EIPHI Graduate School (contract ANR-17-EURE-0002) and supported by Bourgogne-Franche-Comté Region (CONAFLU project). This work has been partly supported by (i) the French research infrastructure ROBOTEX (TIRREX ANR-21-ESRE-0015) and its FEMTO-ST technological facility CMNR and (ii) the French RENATECH network and its FEMTO-ST technological facility.

References

[1] A. Fischer, “The use of monoclonal antibodies in allogeneic bone marrow transplantation,” *British Journal of Haematology*, vol. 83, no. 4, pp. 531–534, 1993.

[2] C. W. Shields, C. D. Reyes, and G. P. López, "Microfluidic cell sorting: a review of the advances in the separation of cells from debulking to rare cell isolation," *Lab on a Chip*, vol. 15, no. 6, pp. 1230–1249, 2015.

[3] V. Gauthier, A. Bolopion, and M. Gauthier, "Analytical formulation of the electric field induced by electrode arrays: Towards automated dielectrophoretic cell sorting," *Micromachines*, vol. 8, no. 8, p. 253, 2017.

[4] A. Lefevre, V. Gauthier, M. Gauthier, and A. Bolopion, "Closed-loop control of particles based on dielectrophoretic actuation," *IEEE/ASME Transactions on Mechatronics*, 2022.

[5] G. Yoon and J. Park, "Topological design of electrode shapes for dielectrophoresis based devices," *Journal of Electrostatics*, vol. 68, no. 6, pp. 475–486, 2010.

[6] C. Lipp, L. Koebel, R. Loyon, A. Bolopion, L. Spehner, M. Gauthier, C. Borg, A. Bertsch, and P. Renaud, "Microfluidic device combining hydrodynamic and dielectrophoretic trapping for the controlled contact between single micro-sized objects and application to adhesion assays," *Lab Chip*, vol. 23, pp. 3593–3602, 2023.

[7] A. Lefevre, M. Gauthier, P. Bourgeois, A. Frelet-Barrand, and A. Bolopion, "Automatic trajectory control of single cells using dielectrophoresis based on visual feedback," *Lab Chip*, vol. 23, pp. 3683–3693, 2023. [Online]. Available: http://dx.doi.org/10.1039/D3LC00318C

[8] A. Alazzam, B. Mathew, and F. Alhammadi, "Novel microfluidic device for the continuous separation of cancer cells using dielectrophoresis," *Journal of Separation Science*, vol. 40, no. 5, pp. 1193–1200, 2017.

[9] H. Li and R. Bashir, "Dielectrophoretic separation and manipulation of live and heat-treated cells of listeria on microfabricated devices with interdigitated electrodes," *Sensors and Actuators B: Chemical*, vol. 86, no. 2-3, pp. 215–221, 2002.

[10] N. Demierre, T. Braschler, R. Muller, and P. Renaud, "Focusing and continuous separation of cells in a microfluidic device using lateral dielectrophoresis," *Sensors and Actuators B: Chemical*, vol. 132, no. 2, pp. 388–396, 2008.

[11] L. D'Amico, N. Ajami, J. Adachi, P. Gascoyne, and J. Petrosino, "Isolation and concentration of bacteria from blood using microfluidic membraneless dialysis and dielectrophoresis," *Lab on a Chip*, vol. 17, no. 7, pp. 1340–1348, 2017.

[12] P. Gascoyne and J. Vykoukal, "Dielectrophoresis-based sample handling in general-purpose programmable diagnostic instruments," *Proceedings of the IEEE*, vol. 92, no. 1, pp. 22–42, 2004.

[13] X. Hu, P. Bessette, J. Qian, C. Meinhart, P. Daugherty, and H. Soh, "Marker-specific sorting of rare cells using dielectrophoresis," *Proceedings of the National Academy of Sciences*, vol. 102, no. 44, pp. 15 757–15 761, 2005.

[14] K. Khoshmanesh, C. Zhang, F. Tovar-Lopez, S. Nahavandi, S. Baratchi, K. Kalantar-zadeh, and A. Mitchell, "Dielectrophoretic manipulation and separation of microparticles using curved microelectrodes," *Electrophoresis*, vol. 30, no. 21, pp. 3707–3717, 2009.

[15] H. Zhang, H. Chang, and P. Neuzil, "Dep-on-a-chip: Dielectrophoresis applied to microfluidic platforms," *Micromachines*, vol. 10, no. 6, p. 423, 2019.

[16] T. Jubery and P. Dutta, "A new design for efficient dielectrophoretic separation of cells in a microdevice," *Electrophoresis*, vol. 34, no. 5, pp. 643–650, 2013.

[17] H. Sadeghian, Y. Hojjat, and M. Soleimani, "Interdigitated electrode design and optimization for dielectrophoresis cell separation actuators," *Journal of Electrostatics*, vol. 86, pp. 41–49, 2017.

[18] S. Kinio and J. Mills, "Design of electrode topologies for dielectrophoresis through the use of genetic optimization with comsol multiphysics," in *2015 IEEE International Conference on Mechatronics and Automation (ICMA)*. IEEE, 2015, pp. 1019–1024.

[19] ——, "Design of optimal electrode geometries for dielectrophoresis using fitness based on simplified particle trajectories," *Biomedical Microdevices*, vol. 18, no. 4, pp. 1–15, 2016.

[20] C.-H. Han, H. Ha, and J. Jang, "Two-dimensional computational method for generating planar electrode patterns with enhanced volumetric electric fields and its application to continuous dielectrophoretic bacterial capture," *Lab on a Chip*, vol. 19, no. 10, pp. 1772–1782, 2019.

[21] A. Homayouni-Amlashi, L. Koebel, A. Lefevre, A. Mohand-Ousaid, and A. Bolopion, "Topology optimization of the electrodes in dielectrophoresis-based devices," *Computers Structures*, vol. 301, p. 107444, 2024.

[22] M. P. Bendsoe and O. Sigmund, *Topology Optimization: Theory, Methods and Applications*. Springer, Feb. 2004.

[23] M. Albrechtsen, B. Vosoughi Lahijani, R. E. Christiansen, V. T. H. Nguyen, L. N. Casses, S. E. Hansen, N. Stenger, O. Sigmund, H. Jansen, J. Mørk, and S. Stobbe, "Nanometer-scale photon confinement in topology-optimized dielectric cavities," *Nature Communications*, vol. 13, no. 1, p. 6281, 2022. [Online]. Available: https://doi.org/10.1038/s41467-022-33874-w

[24] H. Maruyama, A. Iguchi, Y. Tsuji, and T. Kashiwa, "Topology optimization of optical devices using function expansion method and cma-es," in *2022 27th OptoElectronics and Communications Conference (OECC) and 2022 International Conference on Photonics in Switching and Computing (PSC)*, 2022, pp. 1–3.

[25] A. Thabuis, M. C. Rivera, X. Ren, and Y. Perriard, "Topology optimization of an electromagnet manipulator for 3-d uniform magnetic field generation," *IEEE Transactions on Magnetics*, vol. 59, no. 5, pp. 1–4, 2023.

[26] S. Farzinazar, Z. Ren, J. Lim, J. Kim, and J. Lee, "Thermo-mechanical topology optimization of 3d heat guiding structures for electronics packaging," *Journal of Electronic Packaging*, vol. 144, 02 2022.

[27] R. Ortigosa, J. Martínez-Frutos, D. Ruiz, A. Donoso, and J. C. Bellido, "Topology Optimisation of multilayered Electro-Active Polymers considering nonlinear electromechanics," Jun. 2020, working paper or preprint. [Online]. Available: https://hal.science/hal-02862196

[28] A. Bhattacharyya and K. A. James, "Topology optimization of shape memory polymer structures with programmable morphology," *Structural and Multidisciplinary Optimization*, vol. 63, no. 4, pp. 1863–1887, 2021. [Online]. Available: https://doi.org/10.1007/s00158-020-02784-0

[29] D. Ruiz and O. Sigmund, "Optimal design of robust piezoelectric microgrippers undergoing large displacements," *Structural and Multidisciplinary Optimization*, vol. 57, pp. 1–12, 01 2018.

[30] T. Schlinquer, A. Homayouni-Amlashi, M. Rakotondrabe, and A. M. Ousaid, "Design of piezoelectric actuators by optimizing the electrodes topology," *IEEE Robotics and Automation Letters*, vol. 6, no. 1, pp. 72–79, 2020.

[31] A. Homayouni-Amlashi, T. Schlinquer, A. Mohand-Ousaid, and M. Rakotondrabe, "2d topology optimization matlab codes for piezoelectric actuators and energy harvesters," *Structural and Multidisciplinary Optimization*, vol. 63, no. 2, pp. 983–1014, 2021.

[32] A. Homayouni-Amlashi, O. Sigmund, T. Schlinquer, M. Rakotondrabe, and A. Mohand-Ousaid, "Matlab codes for 3d topology optimization of multi-material piezoelectric actuators and energy harvesters," *Structural and Multidisciplinary Optimization*, vol. 67, no. 9, p. 165, 2024. [Online]. Available: https://doi.org/10.1007/s00158-024-03867-y

[33] A. Homayouni-Amlashi, T. Schlinquer, P. Kipkemoi, J. B. Byiringiro, M. Rakotondrabe, M. Gauthier, and A. Mohand-Ousaid, "Topology optimization of micro piezoelectric actuators and energy harvesters at femto-st institute: summary and matlab code implementation," *Journal of Micro and Bio Robotics*, vol. 20, no. 2, p. 6, 2024. [Online]. Available: https://doi.org/10.1007/s12213-024-00168-x

[34] "A monolithic approach for topology optimization of electrostatically actuated devices," *Computer Methods in Applied Mechanics and Engineering*, vol. 197, no. 45, pp. 4062–4075, 2008.

[35] T. B. Jones, *Fundamentals*. Cambridge University Press, 1995, p. 5–33.

[36] X. Wang, X.-B. Wang, and P. R. Gascoyne, "General expressions for dielectrophoretic force and electrorotational torque derived using the maxwell stress tensor method," *Journal of electrostatics*, vol. 39, no. 4, pp. 277–295, 1997.